Investigation on a High-Frequency Controller for Rotor BVI Noise Alleviation

Alessandro Anobile, Giovanni Bernardini and Massimo Gennaretti

Department of Engineering, Roma Tre University, Via della Vasca Navale 79, 00146, Rome, Italy

(Received 26 November 2013; acepted 12 November 2014)

Among the several sources of acoustic annoyance produced by rotorcraft in operating conditions, blade-vortex interactions (BVIs) capture the interest of much of the current research. This paper deals with the reduction of BVI noise from helicopter main rotors by application of the active twist rotor concept (ATR), exploiting smart materials for twisting blades through higher-harmonic torque loads. An optimal, multi-cyclic, control approach is applied to identify the control law driving the ATR actuation during the occurrence of severe BVI events. Numerical predictions are obtained through a computational tool that is able to predict the aeroelastic response of the rotor blades and the emitted noise in arbitrary steady flight conditions. The approach for the control law identification is described and numerical results concerning aeroelastic and aeroacoustic performance of the controlled rotor are presented to assess the proposed methodology.

NOMENCLATURE

$\mathbf{f}_{aer}, \mathbf{f}_{str}^{nl}$	Forcing terms of linear structural dynamics
$\mathbf{m}$	Generalized ATR torque moments
p'_T, p'_L	Thickness and loading noise
$\mathbf{q}$	Vector of the Lagrangian coordinates
$\mathbf{r}$	Distance between source and observer positions
$\mathbf{u}, \mathbf{z}$	Vectors of control and output variables
$\mathbf{v}$	Flow velocity
$\mathbf{x}, \mathbf{y}$	Observer and source position
G	Unit-source solution of the Laplace equation
$\mathbf{G}_u, \mathbf{G}_z$	Gain matrices
J	Cost function
$\mathbf{M}, \mathbf{C}, \mathbf{K}$	Mass, damping and stiffness matrices
S_B, S_W^N, S_W^F	Body, near wake and far wake surfaces
$\mathbf{T}$	Input-output control transfer matrix
$\mathbf{W}_u, \mathbf{W}_z$	Optimal control weighting matrices
c_0, p_0, ρ_0	Speed of sound, pressure and density of undisturbed medium
τ	Emission time
φ_S, φ_I	Scattered and incident velocity potential
u_n, v_n	Flow and body normal velocity components

1. INTRODUCTION

The acoustic annoyance is one of the critical issues concerning the flight of helicopters. The main rotor plays a crucial role in noise generation, through several aerodynamic phenomena that affect its performance. Among these, blade-vortex interactions (BVIs) are relevant sources of noise. Indeed, BVI noise has an impulsive nature, which is particularly annoying for the human ear and typically occurs when the helicopter is in descent or in slow advancing flight[1,2] (i.e., when it operates near the ground and the community). As a consequence, prediction and control of BVI noise (in terms of magnitude and directivity pattern) are important issues for rotorcraft designers both for civil applications and for improving stealthiness in military missions.

Identification of optimal rotor blade shapes and active controls, as well as a definition of optimal minimum noise descent trajectories are strategies extensively investigated by researchers to reduce the acoustic impact of helicopters on communities. Active control systems are particularly suitable for BVI alleviation, in that severe BVIs occur during low speed flight when more power is available to actuators, as compared to high speed forward flight. Approaches based on higher harmonic blade control have been investigated in detail, both numerically and experimentally in the past literature.[2–5] Specifically, the attention has focused mainly on two types of control systems: the individual blade control (IBC), for which each blade is controlled in the rotating frame through pitch links or flaps, and the so-called higher harmonic control (HHC), which acts on all the blades simultaneously by driving the non-rotating component of the swashplate. The benefits of HHC and IBC in reducing both vibrations and acoustic annoyance have been widely discussed, although some drawbacks emerged. Besides problems related to the increase of weight and complexity of the actuation devices, the way these controllers act for BVI noise reduction often corresponds to an increase in low-frequency noise content and in rotor vibration levels.[2,6] Furthermore, the actuators that are typically used for the conventional active control are characterized by limited frequency bandwidth and high vulnerability of the hydraulic systems. Active materials help to overcome most of these limitations, since they operate through the direct conversion from the electrical signal to the mechanical deformation of the material. This allows low-mass and high-bandwidth actuators thus increasing the ability to control the aeroelastic behavior of the individual blades for cancelling the unsteady high-frequency aerodynamic loads, which are the main cause of rotor noise and vibrations. Indeed, in recent years increasing attention to the application of the smart materials to rotorcraft systems has been paid by the research community.[7–12]

This paper presents an IBC controller relying on active twist rotor (ATR) actuation that is aimed at reducing high-frequency rotor noise aerodynamically generated by BVIs. It is an extended version of the work recently presented by the authors,[13] where the conceptual idea of this active twist BVI-controller has been introduced.

The proposed control strategy relies on high-frequency actuation to generate loads aimed at direct suppression/alleviation of those due to BVI. This approach is different from the more

commonly used ones that apply low-frequency (2 to 6/rev) actuators to alter key factors of BVI phenomena, such as miss-distance and blade-vortex interaction angle.[14] It operates in bounded time slots during blade rotation through small, localized blade torsional moments. This allows the system to evolve unaffected by the controller in the rest of the revolution. In this way, BVI phenomena (and related emitted noise) are altered where they occur, which minimizes the onset of negative by-products effects like, for instance, vibratory hub loads increase. The actuation is driven by a control law identified by an optimal, multi-cyclic control method based on main rotor aeroelastic/aeroacoustic numerical simulations. The control law is synthesized by using as control variables the blade torsional deformations, that are suited for suppressing high-frequency BVI loads. The corresponding ATR actuation torques are determined by the application of a simplified linear blade-torsion aeroelastic differential formulation. A high-frequency, BVI-effects alleviation approach is presented also by Modini et al.,[15] where the control law is determined through numerically efficient two-dimensional parallel-BVI simulations, although not accounting for influence of aeroelastic phenomena. Note that the technological feasibility of the proposed high-frequency controller is still an open issue, although much research is under development in this field.[6] Thus, the goal of this paper is to explore its potential performance, as well as to provide an efficient procedure for synthesis and application of control law.

In the following section, the theoretical formulations implemented in the simulation numerical tools applied for control synthesis and verification are briefly outlined. Section 3 provides a detailed description of the control methodology proposed, and finally Section 4 presents and discusses numerical applications aimed at assessing its capability to reduce BVI-induced blade loads and noise.

2. ROTOR BVI NOISE PREDICTION

The simulation of the acoustic disturbance generated by rotors in BVI conditions is a multidisciplinary task; accurate modelling of blade aeroelasticity and aerodynamics is required to yield the blade surface pressure distribution that, in turn, is the input to an aeroacoustic tool providing the radiated noise. Indeed, blade and wake deformations strongly affect BVI phenomena through the corresponding blade-wake miss distance. However, the prediction of the aeroelastic behavior is of paramount importance for the proposed controller, in that it is based on blades aeroelastic twist response to actuation torques.

The following sections provide a brief outline of the methodologies applied in this work to obtain BVI noise predictions used for synthesis and verification of the proposed controller (an extensive validation of them is available, for instance, in Gennaretti et al.[16] or Bernardini et al.[17]).

2.1. Rotor Aeroelastic Modeling

Aeroelastic responses are obtained by combining a blade structural dynamics model with aerodynamic loads given by a quasi-steady sectional formulation corrected with wake inflow.

Blade structural dynamics is described through a beam-like model. It derives from a nonlinear, bending-torsion formulation valid for slender, homogeneous, isotropic, nonuniform, and twisted blades, undergoing moderate displacements.[18] The radial displacement is eliminated from the set of equations by solving it in terms of local tension, and thus the resulting structural operator consists of a set of coupled nonlinear differential equations governing the bending of the elastic axis and the blade torsion.[19] If present, the effects of blade pre-cone angle, hinge offset, torque offset, and mass offset are included in the model.[20]

The aerodynamic loads are evaluated through the quasi-steady approximation of the Greenberg sectional theory.[21] Three-dimensional, unsteady effects deriving from the wake vorticity are taken into account through the influence of the corresponding wake inflow on the downwash at the blade cross sections. The evaluation of the wake inflow is obtained by the boundary element method (BEM) for the solution of a boundary integral equation approach, suited for the analysis of potential flows around helicopter rotors in arbitrary flight condition.[16]

Coupling blade structural dynamics with aerodynamic loads yields an aeroelastic integro-partial differential system of equations. These are spatially integrated through the Galerkin approach with the description of elastic axis deformation and cross-section torsion as linear combinations of shape functions satisfying the homogeneous boundary conditions. This yields a set of nonlinear, ordinary differential equations of the type

$$\mathbf{M}(t)\,\ddot{\mathbf{q}} + \mathbf{C}(t)\,\dot{\mathbf{q}} + \mathbf{K}(t)\,\mathbf{q} = \mathbf{f}_{str}^{nl}(t,\mathbf{q}) + \mathbf{f}_{aer}(t,\mathbf{q}) + \mathbf{m}(t); \quad (1)$$

where $\mathbf{q}$ denotes the vector of the Lagrangian coordinates, $\mathbf{M}$, $\mathbf{C}$, and $\mathbf{K}$ are time-periodic, mass, damping, and stiffness structural matrices that represent the linear structural terms, while $\mathbf{m}$ denotes the generalized torque moments driving the ATR actuation. Nonlinear structural contributions are collected in the forcing vector $\mathbf{f}_{str}^{nl}(t,\mathbf{q})$, whereas vector $\mathbf{f}_{aer}(t,\mathbf{q})$ collects the generalized aerodynamic forces. Since the aim here is to predict the aeroelastic periodic response during steady flight, the aeroelastic system in Eq. (1) is solved by using the harmonic balance approach.[20,22] It is a methodology suitable for the analysis of the asymptotic solution (as time goes to infinity) of differential equations forced by periodic terms, as in the present case. Because of the presence of nonlinear contributions deriving both from structural terms and from the free-wake aerodynamic loads prediction, the final system has to be solved using an iterative approach. To this aim, the Newton-Raphson procedure is applied. In the iterative loop, BEM boundary conditions and corresponding wake inflow are continuously updated accordingly to actual blade aeroelastic response.

2.1.1. Linearized Blade Torsion Dynamic Response

As mentioned in Section 1, in the control feedback process a simplified aeroelastic model is used to identify the ATR actuation torque moments, as those yielding (rapidly, but with a satisfactory degree of accuracy) the optimal blade torsion deformation indicated by the control law (see Section 3). Specifically, for the aeroelastic inverse problem used in the feedback process to determine the actuation torque moments, a reduced version of Eq. (1) describing only the linear torsion behavior is applied. The resulting simplified aeroelastic formulation for the torsional degrees of freedom, $\mathbf{q}_T$, reads:

$$\mathbf{M}_T(t)\,\ddot{\mathbf{q}}_T + \mathbf{C}_T(t)\,\dot{\mathbf{q}}_T + \mathbf{K}_T(t)\,\mathbf{q}_T = \mathbf{f}_{aer,T}(t) + \mathbf{m}(t); \quad (2)$$

where $\mathbf{M}_T$, $\mathbf{C}_T$, and $\mathbf{K}_T$ represent linear structural and aerodynamic contributions, and $\mathbf{f}_{aer,T}(t)$ denotes generalized aerodynamic torque moments independent on blade deformation.

2.2. Rotor Aerodynamic Solver

As already mentioned, the aerodynamic loads collected in $\mathbf{f}_{aer}$ and $\mathbf{f}_{aer,T}$ are obtained by the spanwise integration of loads from the Greenberg sectional theory.[21] In order to be able to predict BVI occurrence and corresponding aeroelastic effects, a three-dimensional, free-wake inflow correction is used. This wake inflow is evaluated by a boundary integral formulation for potential flows suited for the prediction of strong aerodynamic body-wake interaction phenomena,[16] which is also used to determine the blades pressure distribution to be applied for the prediction of BVI acoustic effects radiation (see Section 2.3).

Considering a potential velocity field such that the velocity is given by $\mathbf{v} = \nabla\varphi$, this formulation assumes the potential field, φ, to be given by the superposition of an incident field, φ_I, and a scattered field, φ_S (i.e., $\varphi = \varphi_I + \varphi_S$). The scattered potential is generated by sources and doublets over the surfaces of the blades, S_B, and by doublets over the wake portion that is very close to the trailing edge from which it is emanated (near wake, S_W^N). The incident potential is due to doublets distributed over the complementary wake region that compose the far wake S_W^F.[16] The wake surface partition is such that the far wake is the only wake portion that may come in contact with blades and generate BVI effects. The incident potential is discontinuous across S_W^F, whereas the scattered potential is discontinuous across S_W^N and is represented by[16]

$$\varphi_S(\mathbf{x},t) = \int_{S_B}\left[G\left(v_n - u_n\right) - \varphi_S\frac{\partial G}{\partial n}\right]\mathrm{d}S(\mathbf{y}) - \int_{S_W^N}\Delta\varphi_S\,\frac{\partial G}{\partial n}\,\mathrm{d}S(\mathbf{y}); \quad (3)$$

where $G = -1/4\pi\, r$ is the unit-source solution of the three-dimensional Laplace equation, with $r = \|\mathbf{y} - \mathbf{x}\|$, while $\Delta\varphi_S$ is the potential jump across the wake surface, known from past history of potential discontinuity at the blade trailing edge through the Kutta-Joukowski condition.[23] In addition, $v_n = \mathbf{v}_B \cdot \mathbf{n}$, with $\mathbf{v}_B$ representing the blade velocity (with inclusion of aeroelastic deformation effects), and $\mathbf{n}$ being its outward unit normal, whereas $u_n = \mathbf{u}_I \cdot \mathbf{n}$, with $\mathbf{u}_I$ denoting the velocity induced by the far wake.

Considering the far wake discretized into M panels, assuming the potential jump to be constant over each panel, and recalling the equivalence between surface distribution of doublets and vortices, the incident velocity field is evaluated through the Biot-Savart law applied to the vortices that have the shape of the panel contours. In order to assure a regular distribution of the induced velocity within the vortex core, and thus a stable and regular solution even in blade-vortex impact conditions, a Rankine finite-thickness vortex model is introduced in the Biot-Savart law.[16] The wake-induced velocity field is applied to evaluate the term u_n in Eq. (3) (and the wake inflow correction for the sectional loads theory), as well as the velocity field from which the wake shape evolution is determined in a free-wake analysis. Note that for an accurate prediction of BVI phenomena, the accurate evaluation of the wake distorted shape is essential, meaning that a crucial role is played by the relative positions between the body and the wake.

In this formulation, the incident potential affects the scattered potential through the induced-velocity, while the scattered potential affects the incident potential by its trailing-edge discontinuity that is convected along the wake and yields the intensity of the vortices of the far wake.[16] Once the potential field is known, the Bernoulli theorem yields the pressure distribution to be provided to the aeroacoustic solver.[24]

2.3. Rotor Noise Radiation

In the aeroacoustic simulation presented here, the noise radiated by rotor blades is evaluated through solution of the well-known Ffowcs Williams and Hawkings (FW-H) equation,[25] which governs the propagation of acoustic disturbances generated aerodynamically by moving bodies.

The boundary integral formulation developed by Farassat known as Formulation 1A[26,27] is a widely-used and computationally efficient way to determine the acoustic field as solution of the FW-H equation, and is particularly suited for the problems examined in this paper. When the velocity of the rotor blades is far from the transonic/supersonic range, it yields the aeroacoustic field as a superposition of a term, p'_T, depending on blade geometry and kinematics (thickness noise), and of a term, p'_L, which is related to the blade airloads (loading noise). These two noise contributions are given by the following integrals evaluated over the actual blade surface, S_B.[26,27]

$$4\pi p'_T(\mathbf{x},t) = \int_{S_B}\left[\frac{\rho_0\dot{v}_n}{r|1-M_r|^2}\right]_\tau \mathrm{d}S(\mathbf{y}) + \int_{S_B}\left[\frac{\rho_0 v_n\left(r\dot{\mathbf{M}}\cdot\hat{\mathbf{r}} + c_0M_r - c_0M^2\right)}{r^2|1-M_r|^3}\right]_\tau \mathrm{d}S(\mathbf{y}); \quad (4)$$

$$4\pi p'_L(\mathbf{x},t) = \frac{1}{c_0}\int_{S_B}\left[\frac{\dot{\tilde{p}}\,\mathbf{n}\cdot\hat{\mathbf{r}} + \tilde{p}\,\dot{\mathbf{n}}\cdot\hat{\mathbf{r}}}{r|1-M_r|^2}\right]_\tau \mathrm{d}S(\mathbf{y}) + \int_{S_B}\left[\frac{\tilde{p}\,\mathbf{n}\cdot\hat{\mathbf{r}} - \tilde{p}\,\mathbf{M}\cdot\mathbf{n}}{r^2|1-M_r|^2}\right]_\tau \mathrm{d}S(\mathbf{y}) + \frac{1}{c_0}\int_{S_B}\left[\frac{\tilde{p}\,\mathbf{n}\cdot\hat{\mathbf{r}}}{r^2|1-M_r|^3}\left(r\dot{\mathbf{M}}\cdot\hat{\mathbf{r}} + c_0M_r - c_0M^2\right)\right]_\tau \mathrm{d}S(\mathbf{y}); \quad (5)$$

where c_0 and ρ_0 are, respectively, the speed of sound and the density in the undisturbed medium, whereas $\tilde{p} = (p - p_0)$, with p_0 representing the undisturbed medium pressure, $\mathbf{M} = \mathbf{v}_B/c_0$, $M = \|\mathbf{M}\|$, and $M_r = \mathbf{M}\cdot\hat{\mathbf{r}}$ with $\hat{\mathbf{r}} = \mathbf{r}/\|\mathbf{r}\|$. In addition, $\dot{\mathbf{n}}$ and $\dot{\mathbf{M}}$ denote time derivatives, respectively, of the outward blade surface unit normal vector and of the local blade velocity Mach vector, as observed in a frame of reference fixed with the undisturbed medium, whereas the notation $[...]_\tau$ indicates that these quantities must be evaluated at the emission time, τ, i.e., the time at which the signal arriving in $\mathbf{x}$ at time t started from $\mathbf{y} \in S_B$.[26,27]

In problems dealing with weakly loaded rotors, the thickness and loading noise are comparable. However, when strongly loaded rotors are examined, the thickness noise contribution tends to be negligible and the acoustic disturbance is dominated by the loading noise. Rotors in BVI conditions fall within this category of acoustic phenomena.

3. CONTROL PROCEDURE FOR BVI NOISE ALLEVIATION

In this section, the optimal control method adopted to identify an ATR control law aimed at reducing BVI noise generated by helicopter main rotors is described.

3.1. Definition of the Control Approach

As already pointed out, the proposed controller relies on higher harmonic blade twist deformations to reduce rotor BVI noise as much as possible. Blade torsion deformations suited for noise alleviation are determined by a closed-loop, multicyclic, and optimal control algorithm, in which the corresponding actuation torques to be applied to the blades are provided by a simplified inverse, aeroelastic problem (see Fig.(1) for a scheme of the controller action).

Prior to control law synthesis, preliminary considerations are useful to identify suitable sets of control (input) variables, $\mathbf{u}$, and of (output) variables, $\mathbf{z}$, to be monitored and controlled. Within helicopter configurations in descent flight, several interactions between blades and wake vortices occur in specific regions of both advancing and retreating sides of the rotor disk.[1] For the work presented here, the control action is focused within a time interval during the retreating blade motion defined through the application of the Hann window, and specific harmonics of the blade torsion deformation in that windowed period are chosen as control variables, $\mathbf{u}$. Furthermore, the output variables, $\mathbf{z}$, which are considered in the controller, are noise harmonics decibels predicted at a microphone suitably located. Specifically, the microphone is positioned at the rear edge of the left skid of the helicopter, which is just below the retreating side region of the disk rotor affected by strong BVI, where the controller is actuated. Akin to the approach followed in a previous work on this subject,[2] the noise harmonics considered in the output vector, $\mathbf{z}$, are those between the 6^{th} and the 17^{th} blade passage frequency that represent the BVI contribution to the noise. Note that, differently to the present analysis, in Patt et al.2 the feedback microphone is located on the right skid, since controller action is mainly focused on advancing side BVI.

3.2. Optimal Control Algorithm

Following an approach already used in the past by several authors[2,28,29] that have dealt with the problem of helicopter noise and/or vibration control, the identification of the control law is achieved through a multi-cyclic optimal procedure that consists of minimizing the cost function, $J = \mathbf{z}^{\mathrm{T}}\,\mathbf{W}_z\,\mathbf{z} + \mathbf{u}^{\mathrm{T}}\,\mathbf{W}_u\,\mathbf{u}$, where $\mathbf{W}_z$ and $\mathbf{W}_u$ are weighting matrices defined to get the best compromise between high control effectiveness and low control effort. Because of the inherently time-periodic nature of the problem, in this control approach $\mathbf{u}$ and $\mathbf{z}$ collect sine and cosine harmonic components of variables, thus disregarding transient evolution effects.

Akin to the standard optimal LQR control method (of which the present approach may be interpreted as the natural extension for application to steady-periodic systems), the minimization of the cost function is obtained under the constraint of satisfying the governing equation of the controlled system. The constraint is given by a simplified linear relationship between control variables and system response, $\mathbf{z}_n = \mathbf{z}_{n-1} + \mathbf{T}_{n-1}\,(\mathbf{u}_n - \mathbf{u}_{n-1})$, where $\mathbf{T}_{n-1}$ is the (gradient) transfer matrix for $\mathbf{u} = \mathbf{u}_{n-1}$, which provides the system response perturbation corresponding to a control input perturbation. It describes the aerodynamic/aeroacoustic behavior of the rotor system, and may be obtained by a set of suited numerical simulations. Then, combining the cost function with the constraint equation and minimizing the resulting cost function yield the following optimal control input:

$$\mathbf{u}_n = \mathbf{G}_u\,\mathbf{u}_{n-1} - \mathbf{G}_z\,\mathbf{z}_{n-1}; \tag{6}$$

where the gain matrices are given by $\mathbf{G}_u = \mathbf{D}\,\mathbf{T}_{n-1}^{\mathrm{T}}\,\mathbf{W}_z\mathbf{T}_{n-1}$ and $\mathbf{G}_z = \mathbf{D}\,\mathbf{T}_{n-1}^{\mathrm{T}}\,\mathbf{W}_z$, with $\mathbf{D} = (\mathbf{T}_{n-1}^{\mathrm{T}}\mathbf{W}_z\mathbf{T}_{n-1} + \mathbf{W}_u)^{-1}$.

Equation (6) has to be used in a recursive way: starting from a given control input and corresponding output, the law of the optimal controller is updated until convergence. This provides a closed-loop controller applicable both in a validation process based on simulations given by the complete aerodynamic/aeroelastic/aeroacoustic model and in real helicopter configurations.

3.3. Efficient ATR Control Synthesis

A drawback in using this local controller lies in the significant computational cost of the gradient matrix evaluation that, in principle, is required at each step of the iterative control process about different values of the control variables (it is worth recalling that, evaluating the gradient matrix means determining sensitivities of the noise emitted with respect to each twist deformation harmonic considered in the control actuation).

To obtain an efficient determination of the matrix $\mathbf{T}_n$, the following procedure is applied: (i) starting from undeformed rotor blades, a set of output vectors, $\mathbf{z}$, is evaluated as open-loop responses to a set of small blade twist deformations (input vector, $\mathbf{u}$); (ii) from this database, a least squares polynomial approximation of the functions relating each output variable to each input variable is determined; (iii) at each step of the iterative control process, each element of the gradient matrix, $T_{ij} = \partial z_i/\partial u_j$, is analytically derived from the identified polynomial forms. Thanks to the least squares approximation applied, the application of the optimal local controller is as fast as that of a global controller (i.e., considering a constant gradient matrix), in that it avoids the numerical evaluation of the gradient matrix at each step of the control process. The final step of the identification of the ATR controller consists of determining the torque moments to be applied to the blade, to get the twist deformations required by the optimal control algorithm. For the sake of numerical efficiency (and feasibility of real-time controller), these are derived from the simplified aeroelastic model presented in Eq. (2). Indeed, for a steady-periodic rotor response, expressing the system matrices, the twist Lagrangian coordinates, and the forcing vector in terms of their Fourier coefficients, and then applying a harmonic-balance approach, it yields an algebraic relation between harmonics of the forcing terms (actuation torque moments, in particular) and the harmonics of the twist variables. Thus, letting the harmonics of the twist variables coincide with the elements of the control variables vector, $\mathbf{u}$, from the Fourier representation of Eq. (2) it is possible to derive the harmonic components of the actuation torque moments. This completes the control feedback that, starting from noise measurements at the rear edge of the left skid provides the ATR actuation moments, as synthetically described in the scheme of Fig. (1), where steps of the control process, as well as data exchanged among them, are illustrated.

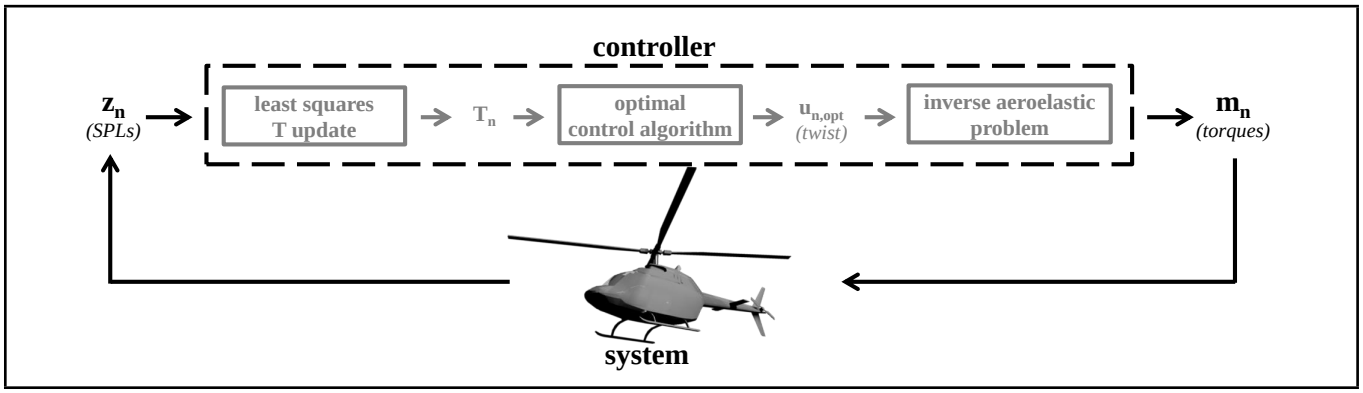

Figure 1. Controller block diagram.

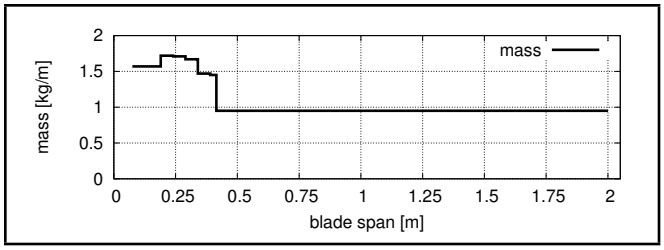

Figure 2. Blade mass distribution.

mode	frequency [Hz]
lag	13.54
flap	20.80
torsion	89.15

Table 1. Blade flap, lag and torsional first natural frequencies of vibration.

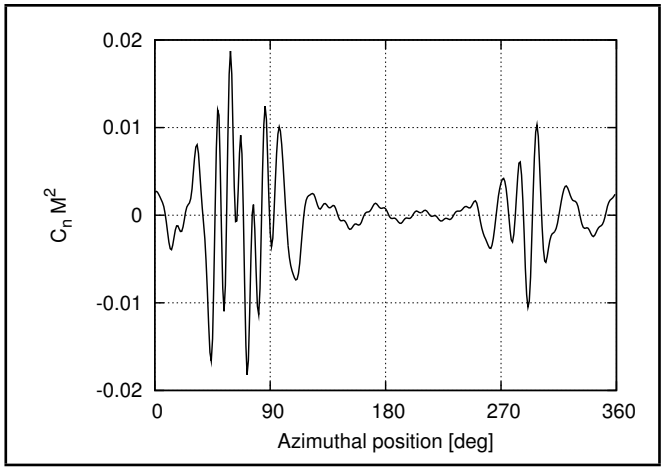

Figure 3. Time history of C_nM^2 high-frequency content ($\geq$ 7/rev), at $r/R = 0.87$.

4. NUMERICAL RESULTS

For validation purposes, the noise control methodology proposed has been applied to a fully hingeless model rotor with a radius $R = 2$ m, that has four blades of constant chord $c = 0.121$ m, a linear twist angle of $-8°$, NACA 23012 section profiles, and a rotational speed $\Omega = 190.12$ rad/s. Blade mass distribution is given in Fig. (2) and blade structural properties are reported in Table 1 in terms of natural frequencies of vibration. The operating condition examined is typically affected by strong BVI events, and consists of a $6°$ descent flight at advance ratio $\mu = 0.15$, with shaft angle $\alpha_S = -5.4°$ (i.e., tilted backwards). The rotor is trimmed with constraints of providing 3300N thrust and null in-plane moments. Free-wake aerodynamic calculations are performed discretizing each blade surface through 15 (upper and lower) chordwise panels and 18 spanwise panels, using 180 azimuth discretization steps, and a 2-spiral wake length.

In the following paragraphs, preliminary studies of the baseline (uncontrolled) case are shown, which allow characterization of the blade's operating conditions and the identification of suited control variables. Then, results concerning two numerical applications of the closed-loop noise control approach are presented, which differ in the aeroelastic tool that provides the rotor feedback to the controller: in the first one, the rotor blades are assumed to have bending stiffness tending to infinity (rigid bending), whereas in the second case the complete, and more realistic, aeroelastic modeling of the rotor blades is considered. From these results, it is possible to assess the effectiveness of the control methodology that was investigated, as well as to estimate the influence of the approximations introduced in the blade aeroelastic modeling applied for control synthesis.

4.1. Preliminary Analysis

Here, investigations aimed at identifying sets of variables $\mathbf{u}$ and $\mathbf{z}$ that are suitable for the control process are presented. Since the purpose of this work is the assessment of the ATR ability to alleviate BVI noise through control of blades high-frequency aeroelastic behavior, an analysis of the blade sectional loads is useful to derive guidelines for the definition of the most appropriate actuation process. In this regard, Fig. (3) presents the time history of the high-frequency content of the C_nM^2 coefficient at the cross section located at $r = 0.87R$ (the frequency content $\geq$ 7/rev has been selected, in that it is strongly affected by BVI events). The figure shows two different blade-vortex interaction occurrences: the most severe in the advancing region, the other appearing in the retreating side.

Hereafter, the ATR control application is focused on the alleviation of the retreating side BVI occurrence. Indeed, it generates effects that are clearly bounded with respect to those due to advancing BVI, and thus provides a well-suited test case for proposed control verification.

The Hann windowing function is applied to the high-frequency content of Fig. 3, in order to highlight the retreating side BVI effects. Figure 4(a) depicts the signal extracted in the azimuth range $\Psi_{ret} = [260°, 320°]$, while Fig. (4(b)) shows the corresponding spectrum related to the windowing period considered, which demonstrates that the dominant BVI

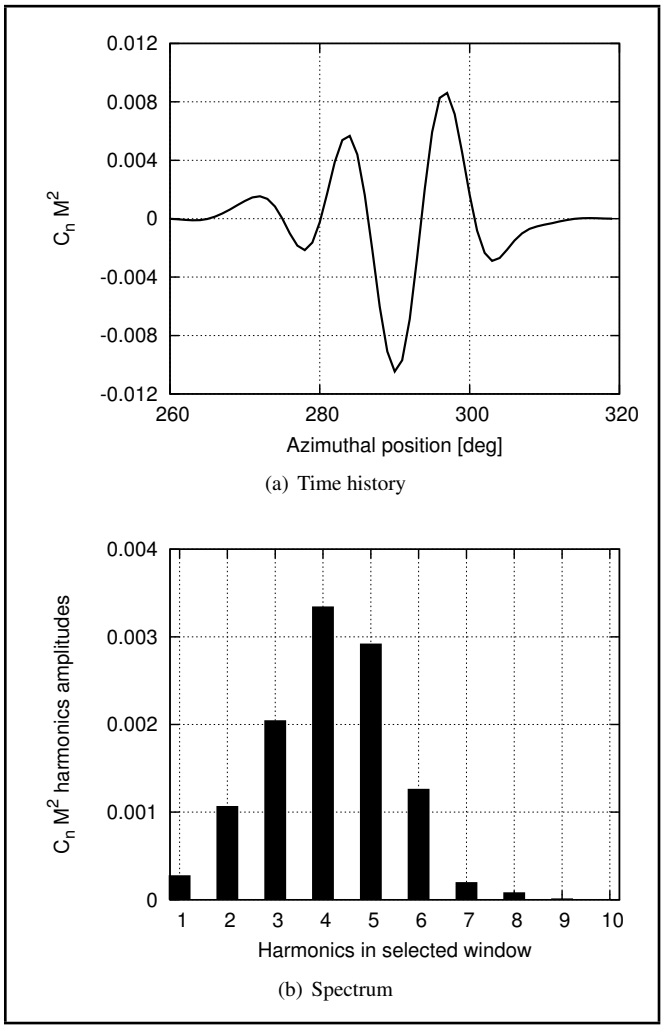

(a) Time history

(b) Spectrum

Figure 4. Windowed $C_n M^2$ high-frequency content.

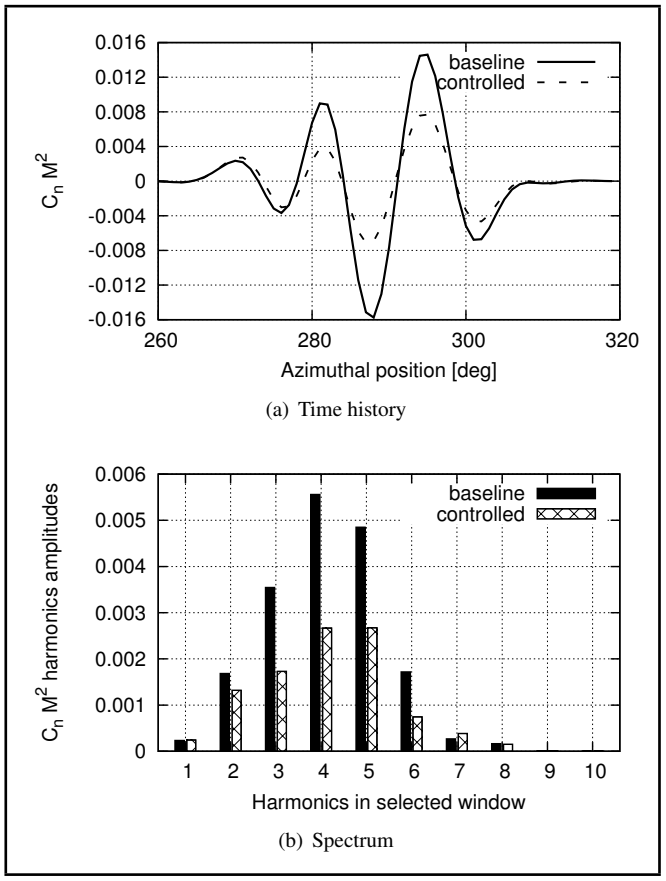

(a) Time history

(b) Spectrum

Figure 5. $C_n M^2$ high-frequency, windowed signal from only-torsion aeroelastic model.

signal harmonics are the 4^{th} and 5^{th} ones (i.e., the 24/rev and the 30/rev, respectively). Considering these results, the sine and cosine components of the 4^{th} and 5^{th} harmonics in $\psi \in \Psi_{ret}$ of the first two blade torsional Lagrangian degrees of freedom, ϕ^I, ϕ^{II}, are assumed as control inputs, $\mathbf{u}$. As mentioned above, the ATR actuation is related to these control inputs through the linearized aeroelastic system in Eq. (2), which yields the torque moment to be applied to the blade in order to get the twist deformations indicated by the optimal control algorithm. In this work, ATR actuation consists of two concentrated torques located at $r_1 = 0.75R$ and $r_2 = 0.90R$, through which it is possible to control the first two blade torsional modes (indeed, their nodes are far from torque locations).

Further, SPLs of the noise signature evaluated/measured at the rear edge of the left skid of the helicopter have been selected as output variables.. Specifically, these are the SPLs of the noise harmonics between the 6^{th} and 17^{th} blade passage frequency, which are strongly affected by BVI; the position of the monitoring microphone has been chosen to be approximately underneath the retreating side of the rotor disk where the controller is actuated.

4.2. Noise Control of Only-Torsion Blades Rotor

First, the closed-loop control is applied to alleviate the noise emitted by the rotor assumed to be composed of blades undergoing only-torsion deformations (i.e., governed by Eq. (2), like for the evaluation of the actuation torque moments). The results from this control application provide highlights on the nominal performance of the controller synthesized, while the effect of a more realistic rotor aeroelastic response to the ATR actuation will be discussed later.

Figure 5 shows an uncontrolled (baseline) and controlled high-frequency content ($>$ 7/rev) of coefficient $C_n M^2$ evaluated at the blade cross section $r = 0.87R$. Time history and spectrum regard the selected azimuth window, Ψ_{ret}, and the controlled signal is that obtained when the control algorithm convergence is reached. This figure demonstrates that a significant reduction of BVI-induced loads is achieved. The corresponding actuated control variables are given in Table 2 in terms of their sine and cosine components. Further, Fig. (6) depicts the effects of control action on blade tip torsion, showing a maximum peak-to-peak difference between controlled and uncontrolled responses of 0.6°, and negligible transient oscillations due to actuation windowing.

Regarding the acoustic effects of control action, the noise emitted on a horizontal plane located 2.3 m below the rotor hub is examined similarly to the analysis presented by Patt et al.[2] Figure 7 shows the noise contour plots predicted from baseline and controlled configurations. The two plots concern the so-called BVISPL, which is evaluated as the Overall Sound Pressure Level (OASPL), but is limited to the noise spectrum between the 6^{th} and the 40^{th} blade passage frequency (i.e., those most affected by BVI events). These figures demonstrate the evident effectiveness of the controller in alleviating the noise generated by the retreating-side BVI occurrence, particularly in the region behind the rotorcraft.

Table 2. Control variables from only-torsion aeroelastic simulation.

variables	ϕ^I_{4C}	ϕ^I_{4S}	ϕ^{II}_{4C}	ϕ^{II}_{4S}	ϕ^I_{5C}	ϕ^I_{5S}	ϕ^{II}_{5C}	ϕ^{II}_{5S}
values [deg]	-0.229	+0.001	+0.024	+0.035	+0.144	-0.048	+0.042	-0.002

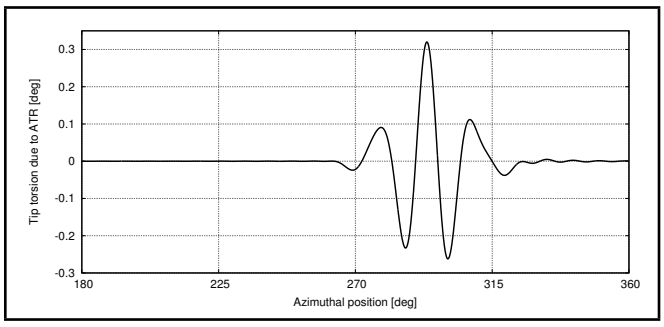

Figure 6. Difference between controlled and uncontrolled blade tip torsion.

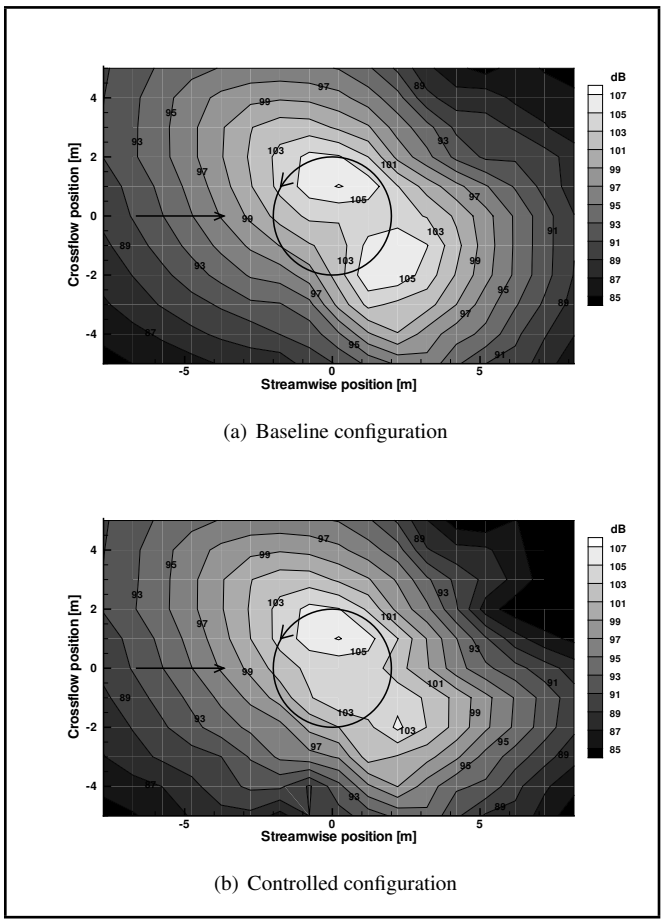

(a) Baseline configuration

(b) Controlled configuration

Figure 7. BVISPL contour plot predicted by only-torsion aeroelastic rotor simulation.

The differences between controlled and uncontrolled noise are presented in Fig. 8(a), where it is evident the presence of a quite large region of noise reduction in the rotor rear side (up to -7dB), whereas noise increase (up to 2.5dB) appears in a limited area close to the rotor retreating side.

Further, Fig. 8(b) shows the difference between controlled and uncontrolled noise in terms of the OASPL, i.e., including also the low-frequency harmonics. In this case, controller effects are smoother than those observed in Fig. 8(a). The noise is generally alleviated with a maximum reduction of about 2dB, while the peak of noise increment (limited to a small region) is equal to 1dB.

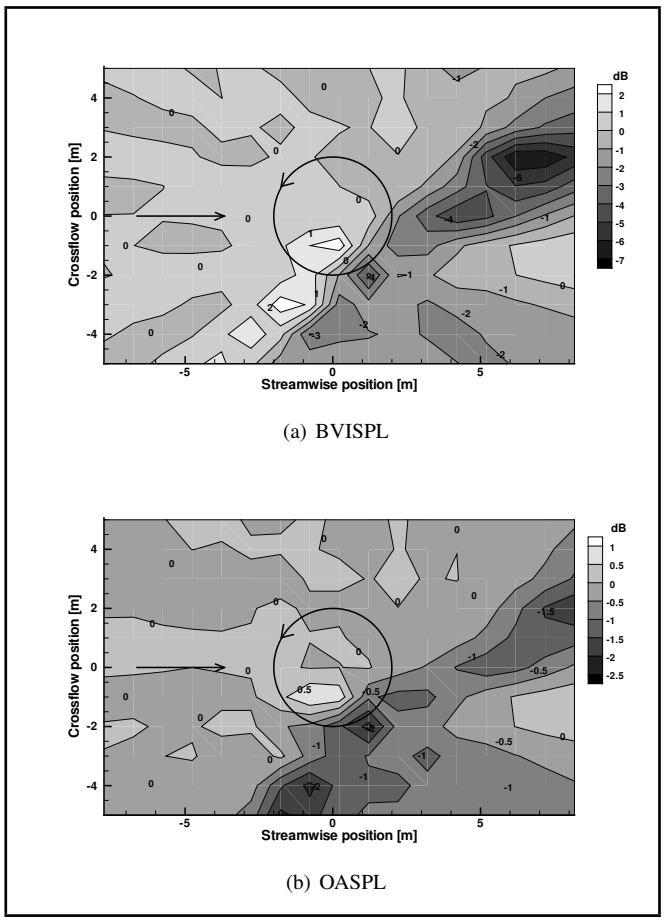

(a) BVISPL

(b) OASPL

Figure 8. Effect of controller on (a) BVISPL and (b) OASPL predicted by only-torsion model.

The effects of the proposed control law on the emitted noise can be considered to be satisfactory by producing reductions of noise levels in most of the examined region. They present a remarkable directivity. Further, it is worth noting that the corresponding aeroelastic response has demonstrated no influence of control actuation on vibratory hub loads transmitted to the airframe, which confirms the advantage of high-frequency controllers in terms of drawbacks onset.

4.3. Noise Control with Complete Rotor Aeroelastic Response

Now, the noise control procedure is applied to a rotor simulated by a complete nonlinear, bending-torsional aeroelastic formulation (see Section 2.1). Unlike the analysis discussed in the section above, here the aeroelastic tool yields a response that may significantly differ from the one that was predicted by the transfer matrix, $\mathbf{T}$, which was used in the controller synthesis. Hence, the following results are a test of proposed control robustness, namely, an assessment of its capability in providing good performance when applied to a system more complex than that used for its synthesis.

Figure 9 shows the high-frequency content of the $C_n M^2$ coefficient for the same blade section and azimuth windowing considered in Section 4.2. Similarly, the controlled signal is

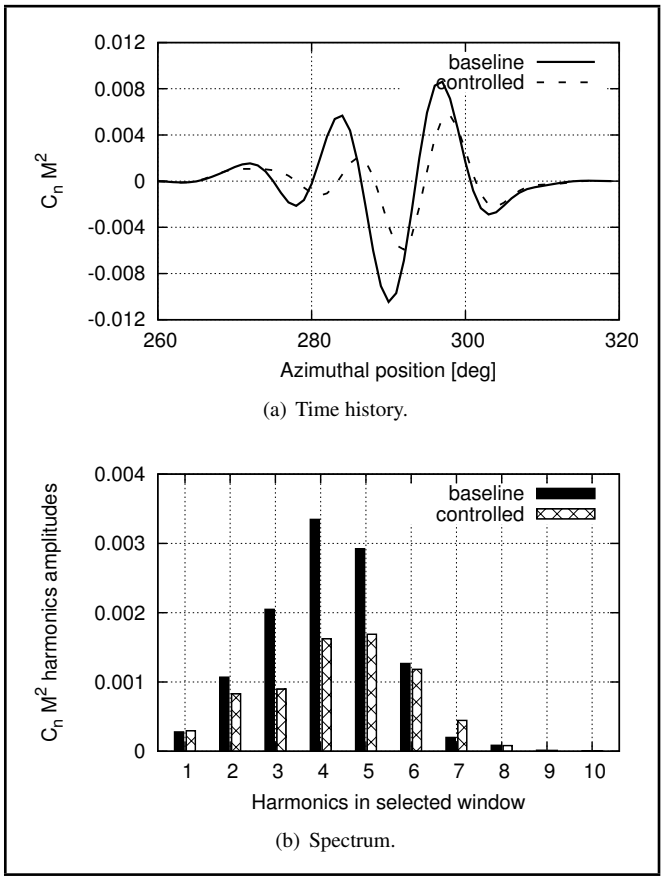

(a) Time history.

(b) Spectrum.

Figure 9. $C_n M^2$ high-frequency, windowed signal from complete aeroelastic model.

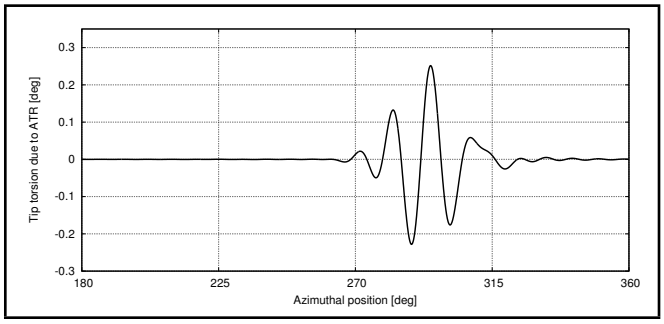

Figure 10. Difference between controlled and uncontrolled tip torsion.

provided at the final step of the iterative control procedure. Then, Fig. 9(b) shows that, for the 4^{th} and 5^{th} windowed load harmonics, alleviations similar to those obtained by the only-torsion aeroelastic model are achieved, although the rest of the harmonics examined are subjected to a smaller reduction. Nonetheless, the overall control effect is still very satisfactory.

In Table 3, the values of the corresponding control variables are given. In this case, the combination of these coefficients gives a maximum peak-to-peak blade tip twist of $0.45°$, showing that good results can also be reached with a smaller control effort. The difference between controlled and uncontrolled blade tip torsion responses is presented in Fig. 10, which shows that also in this case, transient effests due to actuation windowing are negligible.

Next, the effect of the controller on noise alleviation is analyzed in terms of BVISPL contour plots, on the same plane considered in Section 4.2. Figures 11(a) and 11(b) show, re-

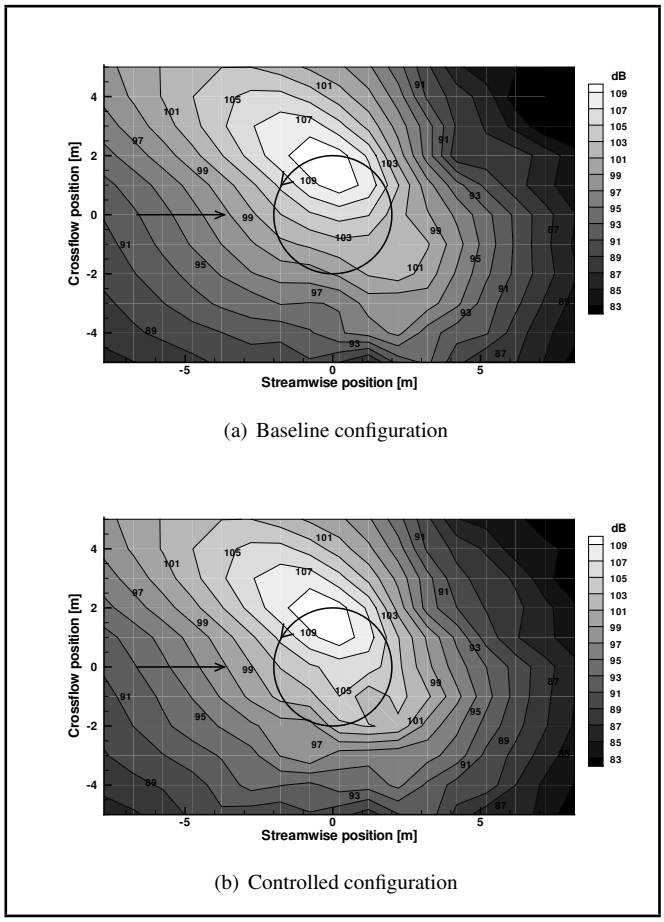

(a) Baseline configuration

(b) Controlled configuration

Figure 11. BVISPL contour plot predicted by complete aeroelastic rotor simulation.

spectively, the acoustic disturbance from uncontrolled and controlled rotor configurations. Compared to the results achieved by the only-torsion aeroelastic model, these figures reveal a lower influence of the controller on the emitted sound, both in terms of noise peaks and directivity modification. This appears more clearly in Fig. 12(a), which highlights the differences between the BVISPL distribution emitted by controlled and uncontrolled configurations. In this case, the maximum reduction of the BVISPL is about 2.7dB, whereas the BVISPL increase is greater than the one from the only-torsion model, which reached 3dB in a limited portion of the observed region. Further, Fig. 12(b) shows the control effectiveness in terms of differences between the OASPL distributions. This plot reveals that the inclusion of low-frequency acoustics tends to reduce peaks and the extent of the region where noise is increased; in this case, peaks of both augmented and alleviated noise are close to about 1.5dB. In terms of vibration levels, also in this case, no differences have been found between the baseline and controlled configurations, which confirms the results obtained for the only-torsion blades rotor.

The outcomes presented in this section show that the efficiency of the control process proposed decreases when noise simulation is based on the complete rotor aeroelastic behavior. Despite this, blade loads are still considerably alleviated, and a wide area in the vicinity of the rotor disk presents a satisfactory reduction in noise levels.

Finally, note that the computational cost required for implementing the control process (see dashed rectangle of Fig. (1) is less than a tenth of a second for each iterative step, by using a single 1.7GHz AMD core. Observing that in real applica-

Table 3. Control variables from complete aeroelastic simulation.

variables	ϕ^I_{4C}	ϕ^I_{4S}	ϕ^{II}_{4C}	ϕ^{II}_{4S}	ϕ^I_{5C}	ϕ^I_{5S}	ϕ^{II}_{5C}	ϕ^{II}_{5S}
values [deg]	-0.092	-0.019	-0.047	+0.068	+0.040	+0.002	+0.018	+0.008

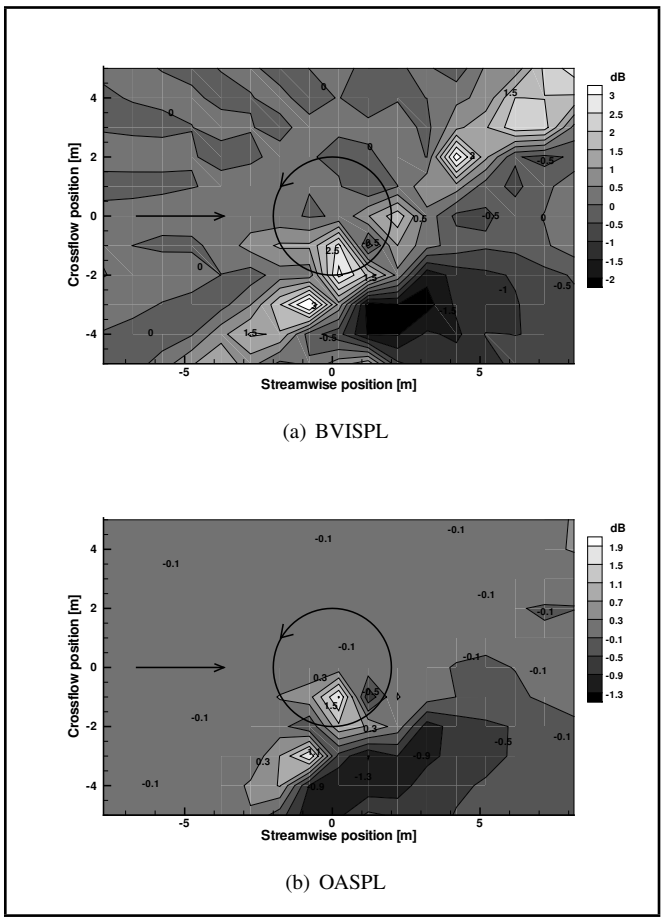

(a) BVISPL

(b) OASPL

Figure 12. Effect of controller on (a) BVISPL and (b) OASPL predicted by complete model.

tions, several rotor revolutions would be taken by rotor systems to reach steady state condition after each step of the iterative control actuation process, and that real scale helicopter rotor revolution periods are significantly longer than that of the examined model, this means that the real time applications of the proposed controller are potentially feasible.

5. CONCLUSIONS

An efficient procedure based on an optimal, multi-cyclic, control algorithm has been proposed and applied for the synthesis of an ATR control law aimed at reducing helicopter rotor BVI noise. Rotor blades have been actuated through localized torque moments in order to drive their twist motion in specific intervals of the blade azimuth location, where the strongest interactions between blades and wake vortices occur. To ensure numerical efficiency and feasibility of a real-time controller, a simplified aeroelastic operator has been applied in the closed-loop actuation process, and the least squares approximation method for identification of the input-output gradient matrix of the local controller has been applied. The main outcomes of the numerical investigation performed are: (1) a preliminary analysis has shown the high-frequency nature of the aerodynamic loads occurring in presence of BVI, thus confirming the need for high-bandwidth actuators (like those relying on smart materials) for providing a direct action to alleviate them; (2) two different closed-loop control actuations have been performed: first, evaluating the rotor aeroelastic response through the simplified only-torsion model, then introducing the complete aeroelastic solver (controlled maximum peak-to-peak blade tip twist of $0.6°$ and $0.45°$ have been obtained, respectively); (3) for both closed-loop control applications, significant reductions of the higher-harmonic loads, as well as noise decrease (up to 7dB for the only-torsion response and 2.7dB for the complete aeroelastic response) in some areas of the acoustic field examined have been obtained; in both cases, increase of the controlled acoustic disturbance ears in a small area located below the rotor retreating side (more than 3dB in the worst case); (4) more relevant BVI noise reductions and directivity pattern changes have been obtained when the simplified response feedback is used; when the complete aeroelastic formulation is used, the increase of the acoustic disturbance below the retreating rotor side becomes higher; (5) both positive and negative effects of the controller on the acoustic field appear mitigated (more than halved) if it is examined in terms of the OASPL, rather than in terms of the high-frequency acoustic content (BVISPL); (6) vibratory levels are observed to be unaffected by control actuation, confirming the advantage of high-frequency controllers in terms of drawbacks onset. (7) the proposed controller is potentially feasible for real-time applications. The findings mentioned above have proven the potentiality of the proposed approach for alleviation of the unsteady aerodynamic loads due to BVIs occurrence, and provide an assessment of its capability in reducing the corresponding emitted noise. They confirm the attractiveness of smart materials for rotorcraft control applications, where low-mass and high-bandwidth actuators are of strong interest. Finally, future development of the proposed control methodology will include its application in reducing advancing side BVI effects, implementing an adaptive control procedure for the high-performance gradient matrix update, and enhancement of control-low synthesis process through application of more efficient blade aeroelastic solvers based on semi-analytic formulations.

REFERENCES

[1] Yu, Y. Rotor Blade-Vortex Interaction Noise. *Progress in Aerospace Sciences*, **36**(2), 97–115, February (2000). http://dx.doi.org/10.1016/S0376-0421(99)00012-3.

[2] Patt, D., Liu, L., and Friedmann, P. P. Simultaneous Vibration and Noise Reduction in Rotorcraft Using Aeroelastic Simulation. *Journal of the American Helicopter Society*, **51**(2), 127–140, (2006). http://dx.doi.org/10.4050/JAHS.51.127.

[3] Yu, Y., Gmelin, B., Splettstoesser, W., Philippe, J., Prieur, J., and Brooks, T. Reduction of Helicopter Blade-Vortex Interaction Noise by Active Rotor Control Technology. *Progress in Aerospace Sciences*, **33**(9-10), 647–687, (1997).

[4] JanakiRam, R. D., Sim, B. W., Kitaplioglu, C., and Straub, F. K. Blade-Vortex Interaction Noise Characteristics of a Full-Scale Active Flap Rotor. *Proc. American Helicopter Society 65th Annual Forum*. Grapevine, Texas, (2009).

[5] Chia, M. H., Padthe, A. K., and Friedmann, P. P. A Parametric Study of On-Blade Control Device Performance for Helicopter Vibration and Noise Reduction. *Proc. 70th Annual Forum of the American Helicopter Society*. Montreal, Quebec, Canada, (2014).

[6] Chen, P. C., Baeder, J. D., Evans, R. a. D., and Niemczuk, J. Blade-Vortex Interaction Noise Reduction with Active Twist Smart Rotor Technology. *Smart Materials and Structures*, **10**(1), 77–85, February (2001). http://dx.doi.org/10.1088/0964-1726/10/1/307.

[7] Chopra, I. Status of Application of Smart Structures Technology to Rotorcraft Systems. *Journal of the American Helicopter Society*, **45**(4), 228–252, (2000). http://dx.doi.org/10.4050/JAHS.45.228.

[8] Chopra, I. Review of State of Art of Smart Structures and Integrated Systems. *AIAA Journal*, **40**, 2145–2187, (2002). http://dx.doi.org/10.2514/2.1561.

[9] Riemenschneider, J. and Keye, S. Overview of the Common DLR/ONERA Project Active Twist Blade (ATB). *Proc. 30th European Rotorcraft Forum*, , (2004).

[10] Thakkar, D. and Ganguli, R. Active Twist Control of Smart Helicopter Rotor - A Survey. *Journal of Aerospace Sciences and Technologies*, , (2005).

[11] Monner, H., Riemenschneider, J., Opitz, S., and Schulz, M. Development of Active Twist Rotors at the German Aerospace Center (DLR). *Proc. 52nd AIAA/ASME/ASCE/AHS/ASC Structures, Structural Dynamics and Materials Conference*, number April, pages 1–10, (2011).

[12] Brillante, C., Morandini, M., and Mantegazza, P. H2 Periodic Control on Active Twist Rotor for Vibration Reduction. *Proc. 70th Annual Forum of the American Helicopter Society*. Montreal, Quebec, Canada, (2014).

[13] Anobile, A., Bernardini, G., and Gennaretti, M. Active Twist Rotor Controller Identification for Blade-Vortex Interaction Noise Alleviation. *Proc. 19th AIAA/CEAS Aeroacoustics Conference*. Berlin, Germany, May (2013). http://dx.doi.org/10.2514/6.2013-2290.

[14] Anobile, A., Bernardini, G., Testa, C., and Gennaretti, M. Synthesis of Rotor BVI Noise Active Controller Through Efficient Aerodynamics/Aeroacoustics Solver. *Proc. 20th AIAA/CEAS Aeroacoustics Conference*. Atlanta, USA, (2014).

[15] Modini, S., Graziani, G., Bernardini, G., and Gennaretti, M. Parallel Blade-Vortex Interaction Analyses and Rotor Noise Control Synthesis. *Proc. 19th AIAA/CEAS Aeroacoustics Conference*. Berlin, Germany, (2013).

[16] Gennaretti, M. and Bernardini, G. Novel Boundary Integral Formulation for Blade-Vortex Interaction Aerodynamics of Helicopter Rotors. *AIAA Journal*, **45**(6), 1169–1176, June (2007). http://dx.doi.org/10.2514/1.18383.

[17] Bernardini, G., Serafini, J., Ianniello, S., and Gennaretti, M. Assessment of Computational Models for the Effect of Aeroelasticity on BVI Noise Prediction. *International Journal of Aeroacoustics*, **6**(3), 199–222, September (2007). http://dx.doi.org/10.1260/147547207782419570.

[18] Hodges, D. and Dowell, E. Nonlinear Equations of Motion for the Elastic Bending and Torsion of Twisted Nonuniform Rotor Blades. *NASA TN D-7818*, , (1974).

[19] Hodges, D. H. and Ormiston, R. A. Stability of Elastic Bending and Torsion of Uniform Cantilever Rotor Blades in Hover with Variable Structural Coupling. *NASA TN D-8192*, , (1976).

[20] Gennaretti, M., Molica Colella, M., and Bernardini, G. Prediction of Tiltrotor Vibratory Loads with Inclusion of Wing-Proprotor Aerodynamic Interaction. *Journal of Aircraft*, **47**(1), 71–79, January (2010). http://dx.doi.org/10.2514/1.41825.

[21] Greenberg, J. M. Airfoil in Sinusoidal Motion in a Pulsating Stream. *NACA TN-1326*, , (1947).

[22] Gennaretti, M. and Bernardini, G. Aeroelastic Response of Helicopter Rotors Using a 3D Unsteady Aerodynamic Solver. *The Aeronautical Journal*, **110**(1114), 793–802, (2006).

[23] Gennaretti, M., Luceri, L., and Morino, L. A Unified Boundary Integral Methodology for Aerodynamics and Aeroacoustics of Rotors. *Journal of Sound and Vibration*, **200**, 467–489, (1997).

[24] Bernardini, G., Serafini, J., Molica Colella, M., and Gennaretti, M. Analysis of a Structural-Aerodynamic Fully-Coupled Formulation for Aeroelastic Response of Rotorcraft. *Aerospace Science and Technology*, **29**(1), 175–184, August (2013). http://dx.doi.org/10.1016/j.ast.2013.03.002.

[25] Ffowcs Williams, J. E. and Hawkings, D. L. Sound Generation by Turbulence and Surfaces in Arbitrary Motion. *Philosophical Transactions of the Royal Society of London*, **264**(1151), 321–342, (1969).

[26] Brentner, K. Prediction of Helicopter Rotor Discrete Frequency Noise - A Computer Program Incorporating Realistic Blade Motions and Advanced Acoustic Formulation. *NASA - TM 87721*, , (1986).

[27] Farassat, F. Derivation of Formulations 1 and 1A of Farassat. *NASA TM 214853*, , (2007).

[28] Zhang, J., Smith, E., and Wang, K. *Active-Passive Hybrid Optimization of Rotor Blades with Trailing Edge Flaps*. PhD thesis, (2001).

[29] Gennaretti, M., Colella, M. M., and Bernardini, G. Analysis of Helicopter Vibratory Hub Loads Alleviation by Cyclic Trailing-Edge Blade Flap Actuation. *The Aeronautical Journal*, **113**, 549–556, (2009).